scientific reports

Check for updates

OPEN

Dual-band transparency over near-IR and THz in surfactant-free DNA solid film

Hayoung Jeong[1], Seunguk Cheona[2], Yong Soo Lee[3], Marjan Ghasemi[2], Soeun Kim[4], Chul Kang[4], Inhee Maeng[5], Seongjin Hong[6] & Kyunghwan Oh[2]✉

We thoroughly investigated the optical properties of surfactant-free deoxyribonucleic acid (SF-DNA) solid films across a broad spectral gamut from ultraviolet (UV) to terahertz (THz). Demonstrating potential as a transparent dielectric material, SF-DNA films could potentially form optical elements, such as lenses, prisms, and waveguides, for dual-band, near-IR and THz applications. SF-DNA films were classified according to their thickness. Nanometer scale films, ranging from 40 to 200 nm, were created by employing spin coating techniques with aqueous DNA solutions on silicon or fused silica substrates. Micrometer scale films, ranging from 1 to 300 µm, were formed as freestanding DNA films using drop-casting methods. Additionally, we have achieved the successful fabrication of an SF-DNA solid cylinder, positioned between two optical fiber ends, featuring a diameter of 100 to 110 µm and an axial length of 65 to 200 µm. SF-DNA films exhibited a unique dual-band transparency in the near-IR spectral range of 1260 to 1870 nm, and in the terahertz range of 0.22 to 0.64 THz. The refractive index dispersion of nanometer-scale films and their birefringence were also measured in the range of 400 to 2,600 nm. The systematic analysis of optical characteristics from UV to THz wavelengths will serve as a critical foundation for further applications of SF-DNA films in the photonic and optoelectronic device fields.

Since the landmark discovery of the double-helix molecular structure of deoxyribonucleic acid (DNA)[1] by Watson and Crick, DNA has served as a cornerstone in a myriad of interdisciplinary scientific explorations. Recently, thin solid DNA films have begun to make significant contributions to optoelectronic applications, with usage scenarios including dye-doped optical amplifiers[2,3], femtosecond pulse laser generation through nonlinear saturable absorbers[4], electron blocking layers in organic light-emitting diodes (OLEDs)[5,6], a cladding layers for polymeric electro-optic waveguide modulators[7], an electronic functional layer in thin-film transistors[8], and optical-radiation sensors[9,10], to name a few. Despite their utility, most of these applications have relied on hybrid structures where DNA films were embedded within inorganic or polymeric materials, and confined to fairly limited spectral ranges, predominantly in the visible and infrared (IR) regions. Previous studies have typically employed lipid-bound DNA, containing surfactant molecules[11,12] which could inadvertently compromise the inherent biocompatibility of DNA. Recently surfactant-free DNA (SF-DNA) thin solid films have been investigated by using aqueous precursors in spin-coating or drop-casting processes[13–15].

Their thorough investigations of material absorption and the refractive index in wider spectral ranges, including the THz domain, has been very scarce[16–18].

Despite their inherent biocompatibility and potentially high functionalities, the deficiency of this crucial data has impeded the expansion of SF-DNA films into broadband photonic applications.

In this study, we systematically studied the optical properties of SF-DNA thin solid film in a wide spectral range from UV to visible, infrared, and terahertz, for the first time to the authors' best knowledge. We successfully fabricated SF-DNA thin solid films utilizing aqueous precursors[13,14,19]. The film thickness was categorized as 1) the nanometer-scale in the range of 40 ~ 200 nm fabricated by the spin-coating on Si or fused silica substrates, and 2) the micrometer-scale in the range of 1 ~ 300 µm by forming a freestanding film or by forming a DNA cylinder between two silica optical fibers. By measuring transmission, we found that SF-DNA films had unique

[1]Center for Superconducting Quantum Computing System, Korea Research Institute of Standard and Science, Daejeon 34113, South Korea. [2]Photonics Device Physics Laboratory, Department of Physics, Yonsei University, Seoul 120-749, South Korea. [3]Center for Quantum Information, Korea Institute of Science and Technology, Seoul 02792, Republic of Korea. [4]Integrated Optics Laboratory, Advanced Photonics Research Institute, Gwangju Institute of Science and Technology, Gwangju 61005, South Korea. [5]College of Medicine, YUHS-KRIBB Medical Convergence Research Institute, Yonsei University, Seoul 03722, South Korea. [6]Department of Physics, Chung-Ang University, Seoul 06974, South Korea. ✉email: koh@yonsei.ac.kr

dual-band transparency in the near IR range of 1270 ~ 1870 nm and the THz range of 0.22 ~ 0.64 THz, as schematically shown in Fig. 1. The dual-band transparency strongly indicates that SF-DNA solid films can be readily applicable in forming optical elements such as lens, prisms, and waveguides in both IR and THz. This potential would open new SF-DNA film application in IR-THz sensing and imaging.

Subsequent sections of this article delve into the quantitative transmission measurement of SF-DNA films, from UV to terahertz. We further examine their refractive index and birefringence over an expansive spectral range of 400 to 2700 nm and THz. Moreover, we also demonstrate the feasibility of optical fiber compatible device applications by creating SF-DNA solid cylinders between two optical fiber facets.

Surfactant-free DNA solid fabrication processes

Using the surfactant-free DNA (SF-DNA) aqueous solutions, we fabricated thin solid films by optimizing three different processes as schematically shown in Fig. 2. Highly purified salmon DNA powder commercially available from Ogata Research Laboratories Ltd.[10,20] in Japan, was dissolved in high purity deionized water to prepare a homogeneous aqueous solution of 0.4 to 2.0 wt. %. To confirm the high purity of DNA, we measured the absorbance A at $\lambda = 230$, 260, and 280 nm to estimate relative ratios such as A_{260}/A_{280} and A_{260}/A_{230} of the prepared solutions. The ratio, A_{260}/A_{280}, has been used as an indicator for the degree of protein contamination while A_{260}/A_{230} for the humic acid contaminants[21]. The absorbance ratio A_{260}/A_{280} and A_{260}/A_{230} for our solutions were in the range of 1.85 ~ 1.9 and 2.2 ~ 2.3, respectively, which ensured the high purity of the prepared DNA solutions[22,23]. The spin-coating process for films with the nanometer-scale thickness is shown in row [A] Fig. 2(b)-(e). The film thickness was flexibly controllable from 40 to 200 nm by varying the DNA concentrations and spinning speed. The drop-casting process is summarized in row [B] Fig. 2(f)-(h), and we obtained freestanding films with a thickness range from 1 to 300 μm by varying the solution volume and the DNA concentration. We further developed a new technique to fabricate an SF-DNA cylinder sandwiched between two silica optical fibers, shown in a row [C] Fig. 2(i)-(k). Optical fibers play a key role in our study, as they are used to create and test the unique optical properties of SF-DNA. These thin, flexible strands of glass or plastic transmit light with minimal loss and are widely used in communication and sensing applications. The length and diameter of SF-DNA cylinders were flexibly varied by controlling the solution volume, the DNA concentration, and the gap between the optical fibers.

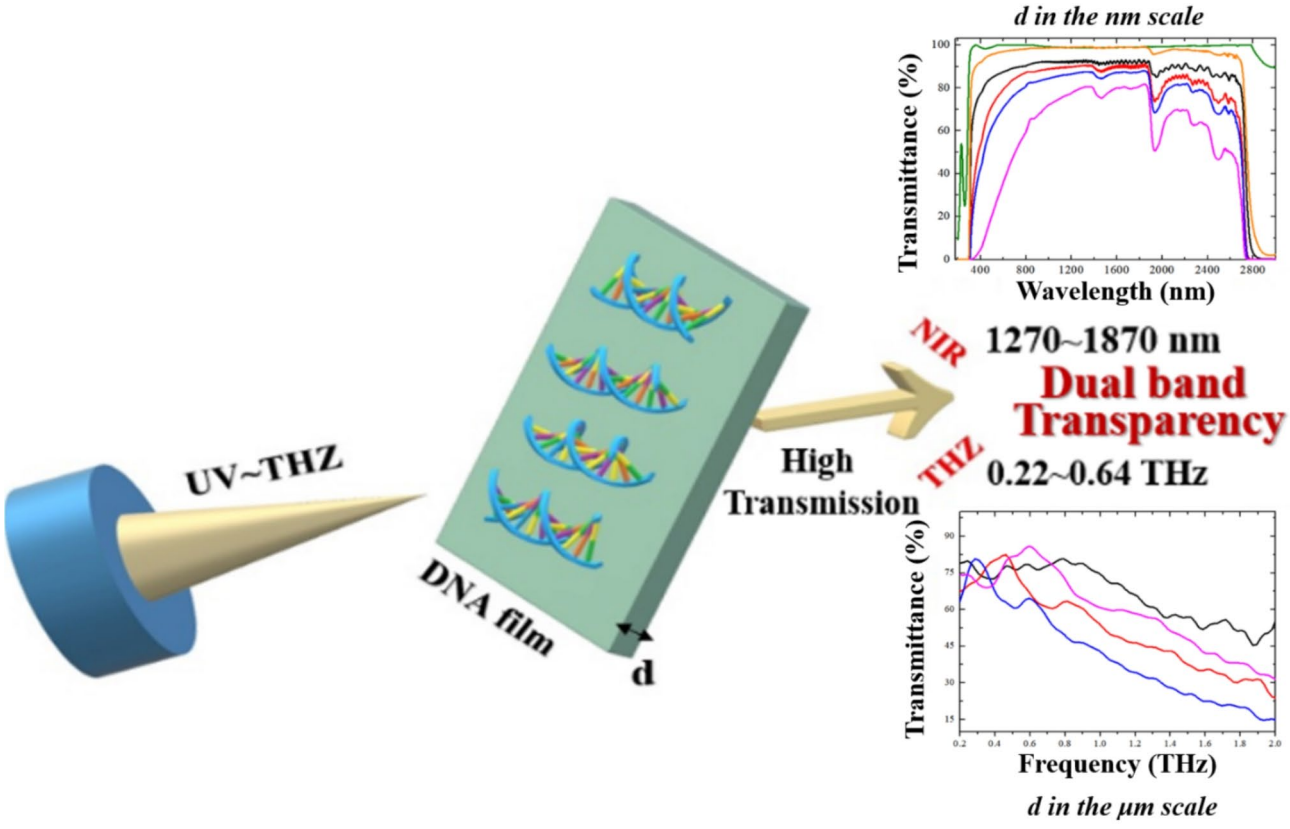

Fig. 1. Schematic diagram of the dual-band transparency in surfactant-free (SF) DNA films. We observed a high transmission in the near-IR region in nanometer-scale thickness films, as in the top-right figure while the micrometer-scale DNA films showed a high transmission in the THz range as in the bottom-right figure, to confirm the dual-band transparency.

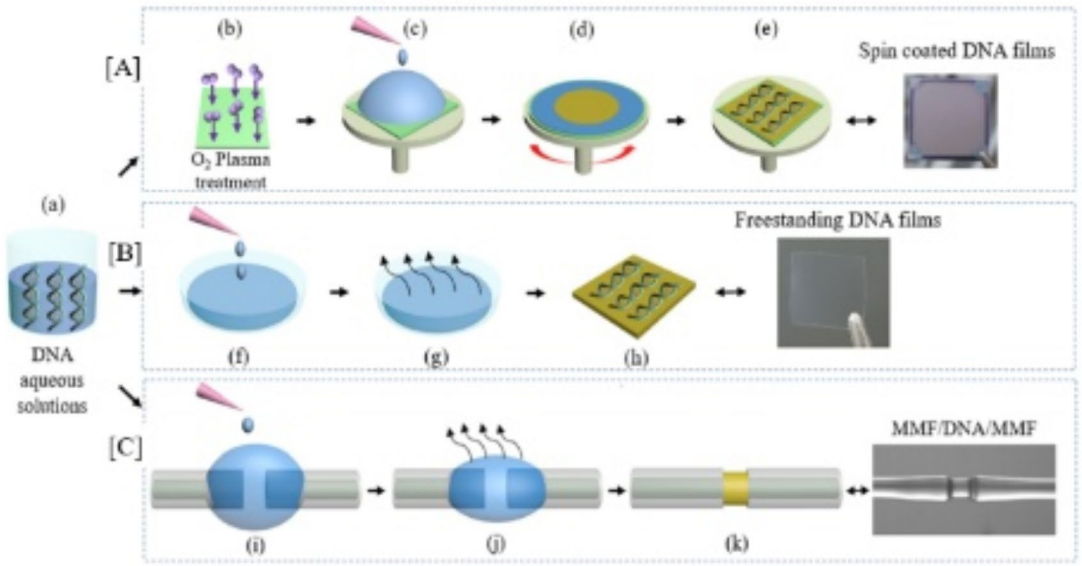

Fig. 2. Fabrication processes of SF-DNA thin solid films using (a) SF-DNA aqueous solution. [A] Spin-coating process: (b) O2 plasma treatment of the substrate surfaces. (c) Dispensing the solution on the substrate. (d) Spinning and solidification by water evaporation. (e) SF-DNA thin solid film on the substrate dried in an oven. [B] Drop-casting process: (f) Dispensing the aqueous solution onto a petri dish. (g) Drying and solidification by water evaporation in a dry oven. (h) Peeling off freestanding films. [C] Cylindrical waveguide fabrication: (i) Dispensing the aqueous solution between the cleaved optical fiber facet (j) Drying and solidification by water evaporation in an oven. (k) Fabricated DNA waveguide sandwiched between two silica optical fibers.

For the spin-coating process in row [A], we firstly optimized the O_2 plasma process to treat the surface of the substrates, p-type Si(100) wafer, and fused silica to facilitate the wetting of the DNA aqueous solution on the surface[24,25]. DNA aqueous solution was dispensed over the surface-treated substrate of a size of 2×2 cm^2, which was then spun at 800 rpm using a commercial spin coater (ACE-200) for 5 min to form a uniform thin film layer. These samples were then dried in a vacuum oven for 24 h at 30 °C to remove the residual water further. We could control the film thickness from 40 to 200 nm by varying DNA concentration from 0.4 to 1 wt. %. SF-DNA films on Si wafer were used for ellipsometry experiments to investigate the refractive index dispersion in the visible and IR, while films on the silica substrates for transmission measurements in UV, visible, and IR spectral range.

To obtain the micrometer-scale thickness of SF-DNA film, we optimized the drop-casting method[15] by dispensing a certain volume of the DNA aqueous solution onto a Teflon petri dish, which was a very hydrophobic surface to facilitate easy peeling-off of the solid film. See row [B] in Fig. 2. The sample was dried at ~ 30 °C in a vacuum oven for ~ 48 h to evaporate water contents and remove air bubbles slowly. The freestanding film was then peeled off and used for transmission measurements in IR, THz spectral range, and FT-IR measurements. The thickness of freestanding DNA film could be flexibly controlled in the range of 1 to 300 μm by varying the volume of DNA aqueous solution and its DNA concentration. Freestanding films are delicate and their fragility depends on thickness. Films thinner than 5 μm often bend or tear during peeling while those 20 μm or thicker are stronger and form a bulk-like structure making them more durable. The thickness was experimentally measured using a surface profiler (DektakXT, BRUKER) and showed a uniform thickness distribution within 1 cm × 1 cm, which is sufficiently large for optical measurements.

We developed a new process to fabricate a solid SF-DNA cylinder between two optical fiber facets. See row [C] in Fig. 2. Note that most prior DNA thin films have been in the planar form, and only a few cylindrical fibers have been reported using DNA-CTMA[26,27]. The previous techniques have required a tailored tapered

silica fiber tip to draw nano/microfibers from a very dense DNA-CTMA solution. Still, they have not solved the fundamental issue of connecting a conventional single mode fiber with a low loss.

In this study, we proposed and experimentally realized an efficient alternative approach, sandwiching, instead of drawing, for the first time. We prepared a viscous aqueous solution with a high DNA concentration of 2.0wt %. We carefully dispensed its droplet into the gap between two optical fibers' facets mounted on x–y-z micro-positioners. The fibers were cleaved at 90° and aligned along the common axial direction. SF-DNA droplet wetted the fiber facets in the gap and was maintained at 20˚C in a dry N_2 purged environment. The droplet formed a DNA solid cylinder connecting two optical fibers as the water evaporated outward in the gap. The SF-DNA cylinder's diameter and length were controlled by varying the DNA droplet volume and gap distance between two optical fibers. In prior DNA-fiber hybrid composites, DNA film has been deposited only on the end-facet or outer surface of optical fiber that can be used as a biosensor and ultrafast laser pulse generation[4,10,28]. This unique solid DNA cylinder between optical fibers can find various applications in fiber-compatible photonic devices and sensors, which the authors are pursuing.

In the following sections, we will describe the optical characteristics of SF-DNA solid films Fig. 2 over a wide spectral range from UV to THz and discuss the transmission properties of the SF-DNA cylinder sandwiched between optical fibers.

Experimental result

UV–VIS-IR transmission through SF-DNA solid films

We measured transmission spectra of SF-DNA thin films fabricated by both spin-coating and drop-casting in a broad spectral range from $\lambda = 200$ to 3,000 nm covering UV to visible and IR. The measurements were consistently taken using commercial spectrometers (Cary5000, Agilent) and the results are summarized in Fig. 3. We varied the SF-DNA film thickness from 0.2 to 150 μm by choosing the appropriate fabrication processes Fig. 1. The 200 nm thickness sample was fabricated using the spin-coating on a fused silica substrate, and the 8 μm thickness film by drop-casting. Larger thickness of 27, 50, 71, and 150 μm were all freestanding films fabricated by the drop-casting process using a Teflon petri dish. DNA strongly absorbs the ultraviolet region from 200 to 380 nm due to electronic transitions of aromatic bases of nucleic acids[29]. The IR absorption of 2,700 ~ 3,300 nm corresponds to the stretching frequency of OH bond[16]. Fringes in the transmittance spectra are attributed to multiple reflections from the film's surface[15,23]. We found additional absorption bands: 1400 ~ 1520 nm, 1890 ~ 2020 nm, 2230 ~ 2310 nm, and 2420 ~ 2520 nm, whose absorbance were much lower than those of the UV electronic transition and the OH bond stretching. The absorbance of those bands monotonically increased with the film thickness or the DNA concentration. In the nanometer-scale thin films, these bands were negligible to result in a high transparency in all NIR regions except for absorption band by stretching of OH bond. See the green curve in Fig. 3. These bands could be attributed to combined results of vibration of biomolecules consisting of DNA, protein, and residual H_2O molecules that remained within the films[30,31]. However, DNA films were all processed in a vacuum oven for more than 24 h, H_2O molecules present within DNA film would not be sufficiently high to dominate the IR spectra. The absorbance A_{260}/A_{280} ratio of the prepared DNA solution indicated that the percentage of protein was negligible compared to prior DNA specimens[15]. Therefore, we attribute the above absorption band mainly to the vibration of biomolecules consisting of DNA[32–34].Note that

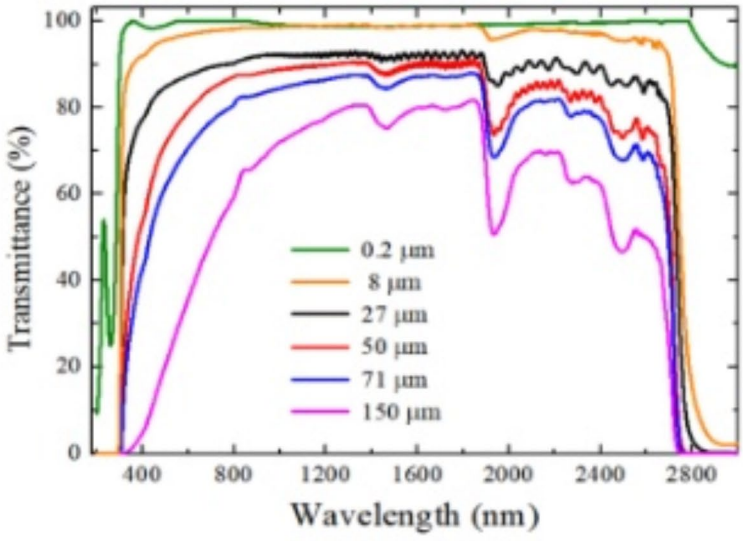

Fig. 3. UV-Visible-NIR transmittance spectra of SF-DNA films for various film thicknesses.

all DNA films in Fig. 3 showed a high transmittance of over 80% in the spectra range of 1260 nm ~ 1380 nm and 1580 nm ~ 1870 nm, serving as a transparent window.

Refractive index measurements of DNA films from UV to NIR

To measure the refractive indices of nanometer-scale SF-DNA films on Si substrate, we used variable-angle spectroscopic ellipsometry (VASE Woollam) that can cover the spectral range from $\lambda = 380$ to 2700 nm. Since the humidity strongly influences the birefringence of DNA films[15], we conducted the experiments under the same humidity condition of ~ 25% at 20 °C. We estimated the refractive indices using the Sellmeier model[35,36] because there were no prominent absorption bands in the spectral range, as shown in the green curves of Fig. 3. Figure 4 summarizes n_{TE}, the refractive index for the polarization with the electric field parallel to film surface, and n_{TM}, for the polarization with the electric field perpendicular to film surface, for SF-DNA films with the thickness of 42 and 137 nm. Here, we confirmed that our measurement of $n_{TE} = 1.523 \sim 1.540$, $n_{TM} = 1.546 \sim 1.569$ at $\lambda = 633$ nm were consistent with prior reports[4,15], which ensures the validity of our experiments in the extended the spectral range over $\lambda > 2500$ nm.

We found a significantly large birefringence (n_{TM}—n_{TE}) in the nanometer-scale SF-DNA films, which depended on the film thickness. The birefringence was plotted as a function of wavelength in Fig. 5. In Fig. 5(a), we found that the 42 nm thickness film showed an order of magnitude lower birefringence than the thicker film with the thickness of 137 nm in Fig. 5(b). Birefringence monotonically increased with the wavelength, saturating at $\lambda > 1500$ nm in both films. As the film thickness increased to 137 nm, the birefringence was as high as 0.0375 ~ 0.0510, which indicates that the double helixes of DNA were aligned more parallel to the substrate surface[37–39]. As we further increased the film thickness, however, we did not observe an increase in the birefringence, indicating DNA alignment in a thin solid film saturated within the thickness of ~ 100 nm. The refractive index in the direction parallel to the nucleobase pairs is larger than that along the double helix axis due to the highly anisotropic polarizability of the π electrons in the nucleobases[40]. The birefringence of SF-DNA films could be attributed to the molecular-level anisotropy in the refractive index of DNA and the surface interaction between the films and the substrate[41].

Transmission through cylindrical DNA waveguide between two optical *fiber* facets

We developed a process to fabricate a cylindrically symmetric DNA waveguide using the hydrophilic surfaces of the cleaved silica fibers as described in Section "Surfactant-free DNA solid fabrication processes" and the row [C] in Fig. 2. Figure 6 shows the optical microscope image of the SF-DNA cylinder sandwiched between two optical fibers. We used commercial silica multimode optical fiber (MMF) with a core diameter of 62.5 μm and an outer cladding of 125 μm. The refractive indices of the silica-based multimode optical fiber (MMF) used in our experiments are approximately 1.447 for the core and 1.444 for the cladding at a wavelength of 1550 nm.

Since we dispensed the DNA solution between the two optical fibers using a syringe, the solution overfilled the gap and adhered to the outer surface of the optical fibers, which made a kind of taper, as shown in Fig. 6. The diameter of the DNA waveguides at the gap was in the range of 100 ~ 110 μm. Note that the SF-DNA cylinder served as the core and the surrounding air as the cladding to form a sequentially concatenated [silica MMF]-

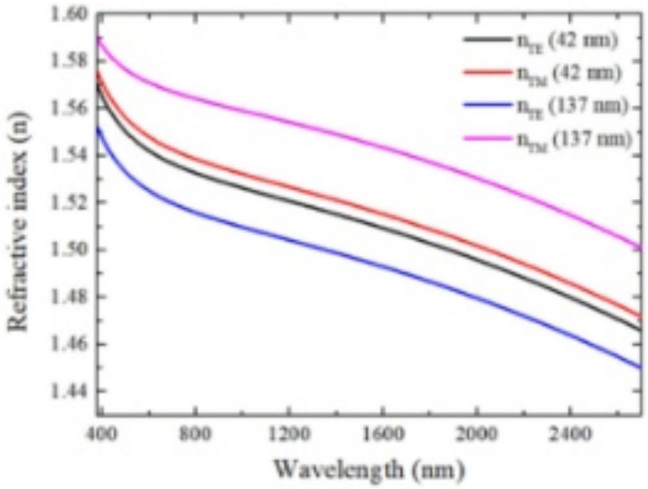

Fig. 4. Refractive index of nanometer-scale spin-coated SF-DNA thin solid films with a thickness of 42 nm and 137 nm in the visible to NIR regions. Here we used the Sellmeir fitting for the ellipsometry measurements.

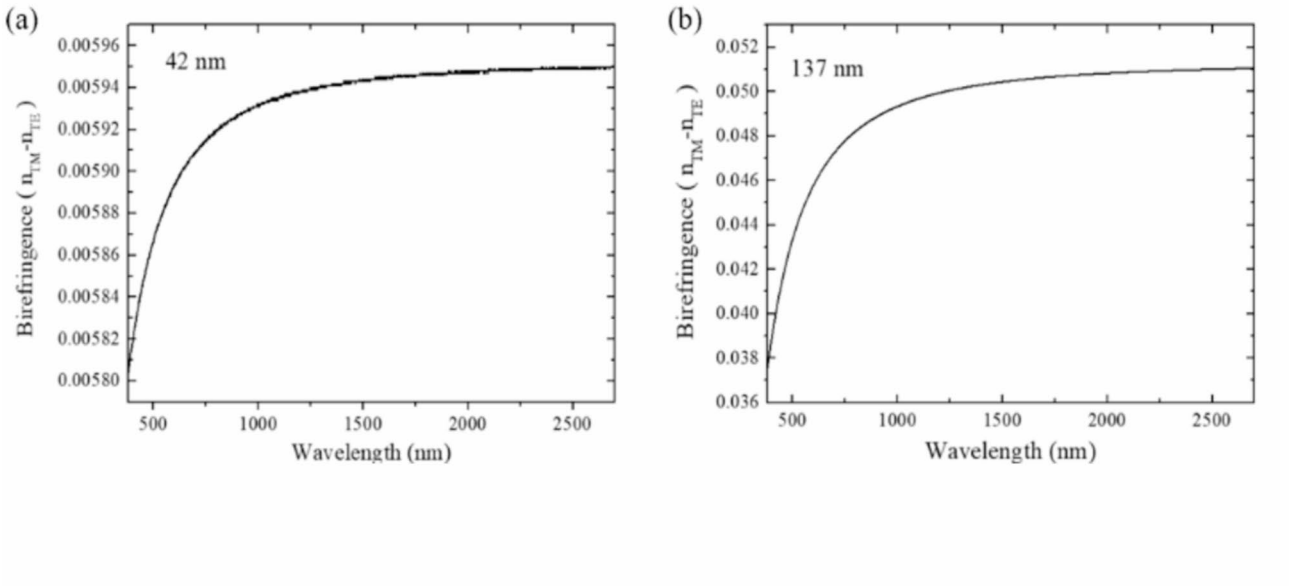

Fig. 5. Birefringence dispersion of nanometer-scale spin-coated SF-DNA solid thin films with a thickness of (a) 42 nm, (b) 137 nm.

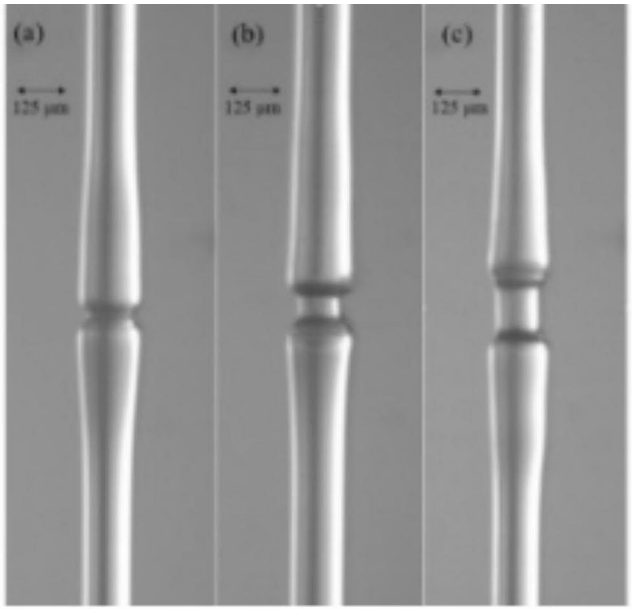

Fig. 6. Optical microscope images of the DNA cylindrical waveguides connecting cleaved facets of multimode fiber. The diameter of DNA cylindrical waveguide was in the range of 100 ~ 110 μm and their lengths were (a) ~ 65 μm, (b) ~ 115 μm, (c) ~ 200 μm.

[SF-DNA MMF]-[silica MMF] structure. To measure propagation loss through the concatenated waveguide, we used a white light source (ANDO AQ4303C) and an optical spectrum analyzer (HP Agilent 86142A) in the wavelength range from 1200 to 1600 nm. The results are shown in Fig. 7 with a 6.7 ~ 10.5 dB/mm propagation loss. This value is comparable to previously reported DNA waveguides[42–44]. It is noted that the propagation loss in the SF-DNA cylinder was consistent with the transmittance spectra in Fig. 3, such that it also showed a lower value in the NIR window of the SF-DNA films. Therefore, the propagation loss was attributed mainly to the material absorption of DNA solid film. And mismatch between SF-DNA MMF and silica MMFs in the diameter and the refractive index also contributed to the loss. This unique [silica MMF]-[SF-DNA MMF]-[silica MMF] structure can be readily applied to various biochemical sensing, which will be reported in separate papers by the authors.

FT-IR measurement of micrometer-scale DNA films

Using a commercial Fourier transform infrared (FT-IR) spectroscopy system (Vertex 70, Bruker), we investigated the transmission of the micron-scale SF-DNA films in the wavelength range from 3 to 25 μm. Here we used freestanding DNA solid films with thicknesses from 5 to 65 μm, and the results are summarized in Fig. 8. Peaks in FTIR absorption spectra of SF-DNA films represent the vibrational resonance frequencies of constituents such as nucleobases, sugar, phosphate groups, and OH stretching[16,45].

Note that the spectral positions of those bands did not change with the film thickness, which strongly indicates the molecular structures of micrometer-scale SF-DNA films were nearly identical. Yet, the overall transmittance significantly decreased as the DNA film thickness increased beyond 25 μm. Transmittance in the mid-IR spectral range $6\ \mu m \leq \lambda \leq 20\ \mu m$ rapidly converged to zeros for SF-DNA films thicker than 34 μm. From the transmission measurements in the FTIR range of 3 to 25 μm, the absorption coefficient was estimated to be around 184 to 300 cm^{-1} in the high-transmission region of 4.5 to 5.2 μm, and between 1287 and 1714 cm^{-1} in the low-transmission region of 10 to 25 μm.

We confirmed that SF-DNA films provided superior absorption in a wide spectral range of Mid-IR compared with other polymeric materials[46,47], which indicates that DNA films could be applied as Mid-IR blocking layer.

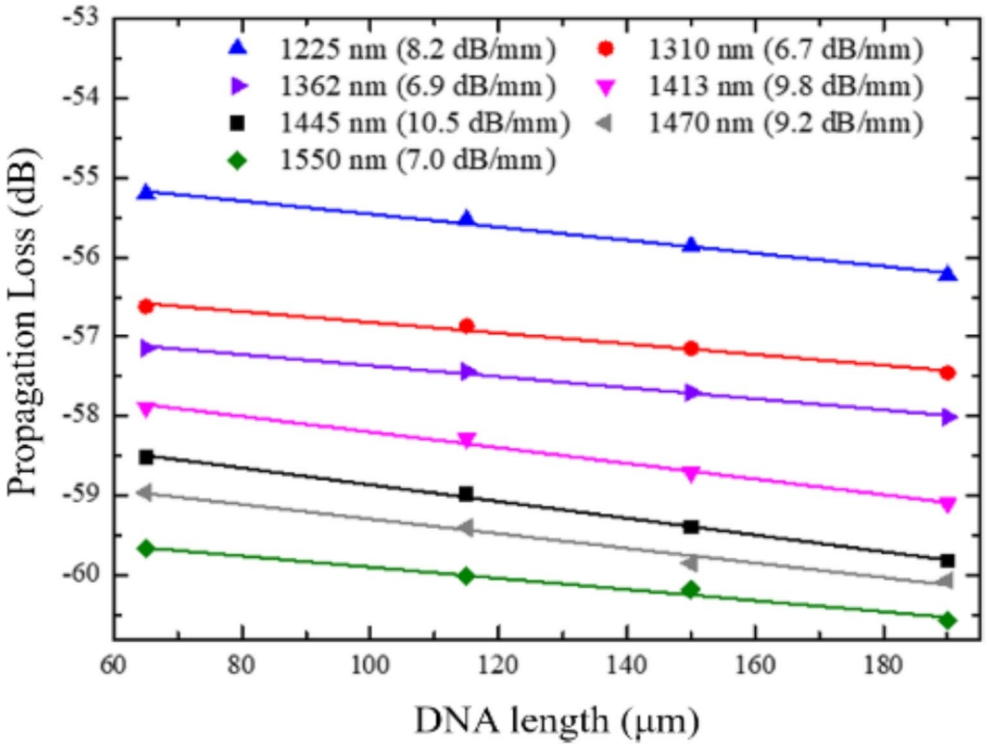

Fig. 7. The propagation loss of [silica MMF]-[SF-DNA MMF]-[silica MMF] waveguide structure for various IR wavelengths.

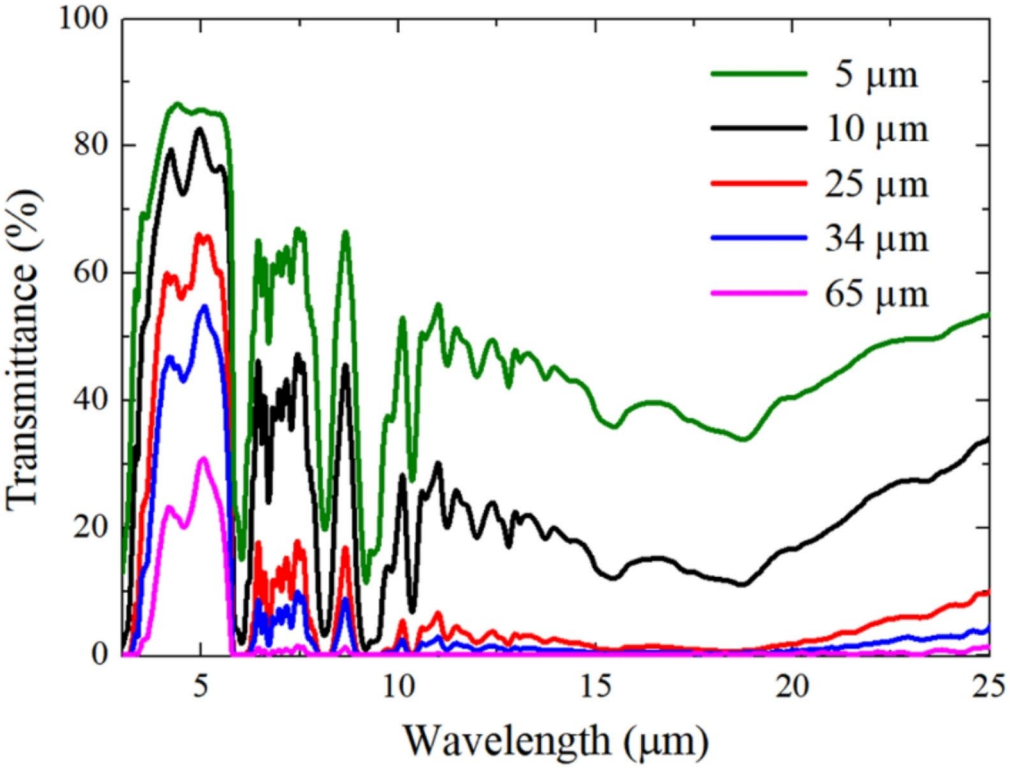

Fig. 8. FT-IR transmittance spectra of micrometer-scale freestanding SF-DNA films.

Terahertz spectroscopy of DNA films

In a longer wavelength beyond the FT-IR range, the transmission of micrometer-scale SF-DNA films were further investigated using a standard THz time-domain spectroscopy (THz-TDS) system[48–50] as schematically shown in Fig. 9. The system used a femtosecond Ti:sapphire laser (Mai Tai, Spectra-physics), with a central wavelength at 800 nm, a pulse duration of ~ 100 fs, and a pulse repetition rate of 80 MHz. The laser was divided into the THz generation and detection arms by a beam splitter. In the THz generation arm, the laser beam was focused on an InAs crystal to generate THz radiation[48]. The THz radiation was collimated and focused using parabolic mirrors to allow measurements in the spectral range from 0.2 to 2.0 THz. The SF-DNA film was located at the focal positions of the parabolic mirrors on both sides. The transmitted pulse signal through the SF-DNA film was detected using a photoconductive antenna. The fast Fourier transform (FFT) of the time-domain signals resulted in the frequency domain signals[45].

We prepared micrometer-scale freestanding DNA solid films, with a thickness range from 94 to 260 μm. We took an average for ten measurements to obtain the results in THz transmission spectra Fig. 10**.**Additionally, since the THz-TDS measurements were performed in a much drier environment with humidity levels around 1%, the absorption of THz radiation due to water vapor was effectively minimized.

Interference fringes were observed due to the multiple reflections at the interfaces of SF-DNA film and the air[51,52]. Notably, high transparency of over 70% in the SF-DNA films was observed in a spectral range of 0.22 ~ 0.64 THz. The corresponding absorption coefficients were 20 ~ 30 cm^{-1}. We also estimated the refractive index n = 1.86 ~ 2.18 in the spectra range of 0.22 THz ~ 2 THz by using the analytical expressions given in terms of the amplitude ratio and the phase difference[53,54]. These values were comparable to those of biomolecule films in previous reports[17,52].

Discussions

In the realm of terahertz (THz) applications, key optical components including lenses, prisms, and waveguides are frequently manufactured from THz-transparent polymers, primarily due to their adaptable fabrication capacities. Among the wide assortment of polymers at our disposal, polymethylpentene (TPX), polyethylene (PE), polypropylene (PP), and polytetrafluoroethylene (PTFE or Teflon) are most commonly employed. These materials, boasting a lower refractive index than other solid-state materials, are pivotal in curtailing Fresnel reflection loss within the THz region.

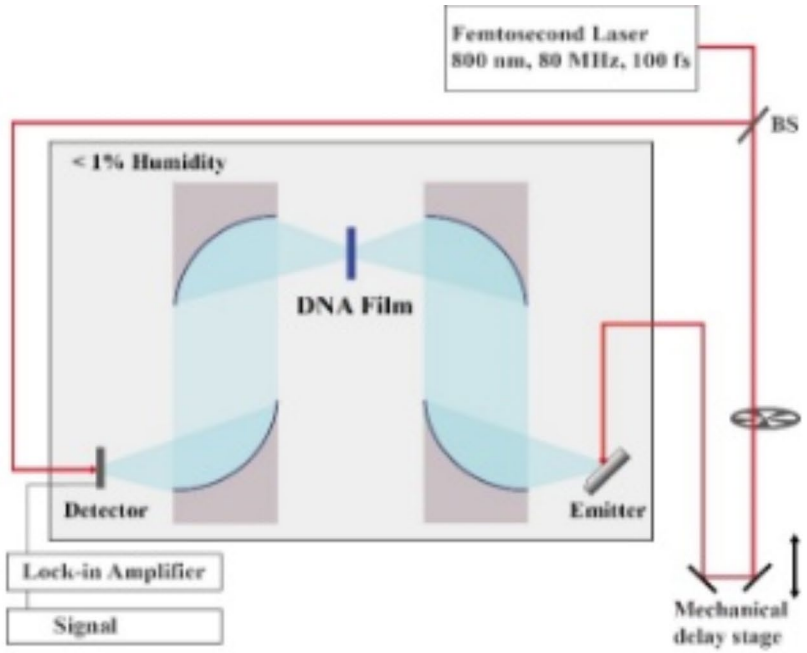

Fig. 9. Transmittance spectra of micrometer-scale freestanding DNA films in the terahertz spectral region.

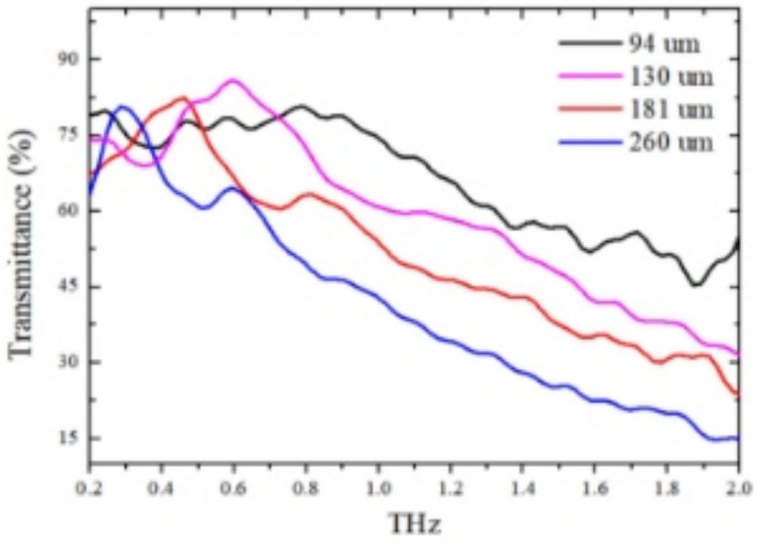

Fig. 10. The schematic diagram for THz-TDS experimental set-up to measure transmission of SF-DNA films in THz.

Material	Spectral range			
	Visible $\lambda = 0.4 \sim 0.7$ µm	**Near-IR** $\lambda = 0.7 \sim 3.0$ µm	**Mid-IR** $\lambda = 3.0 \sim 25$ µm	**THz (0.3 ~ 1.5 THz)** $\lambda = 200 \sim 1000$ µm
TPX [50,51,53]	Good transmission	Good transmission	Absorptive	Good transmission
	$T > 65\%$, $\lambda = 0.4 \sim 0.7$ µm	$T > 70\%$, $\lambda = 0.7 \sim 1.6$ µm	$T < 20\%$, $\lambda = 3.0 \sim 10$ µm	$T > 80\%$, $\lambda = 200 \sim 1000$ µm
	Thickness of 5.08 mm	Thickness of 1.27 mm	Thickness of 5.08 mm	Thickness of 2.0 mm
PTFE [50,52]	Absorptive	Good transmission	Absorptive	Good transmission
	$T < 5\%$, $\lambda = 0.4 \sim 0.7$ µm	$T > 50\%$, $\lambda = 1.5 \sim 3.0$ µm	$T < 20\%$, $\lambda = 8 \sim 9$ µm $T < 20\%$, $\lambda = 15 \sim 20$ µm	$T > 80\%$, $\lambda = 200 \sim 1000$ µm
	Thickness of 200 µm	Thickness of 100 µm	Thickness of 100 µm	Thickness of 100 µm
SF-DNA (This study)	Low transmission	Good transmission	Absorptive	Good Transmission
	$T < 50\%$, $\lambda = 0.4 \sim 0.7$ µm	$T > 75\%$, $\lambda = 1.27 \sim 1.39$ µm $T > 75\%$, $\lambda = 1.58 \sim 1.87$ µm	$T < 10\%$, $\lambda = 6 \sim 25$ µm	$T > 75\%$, $\lambda = 200 \sim 1500$ µm (0.2 ~ 1.5 THz)
	Thickness of 150 µm	Thickness of 150 µm	Thickness of 34 µm	Thickness of 94 µm

Table 1. The transmittance of TPX, PTFE, and DNA in the visible, Near-IR, Mid-IR, and Terahertz The values in the table were taken from the corresponding references for TPX and PTFE, and Figs. 3, 8 and 10 in this study.

A comparative analysis of TPX and PTFE[55–58] against our proprietary SF-DNA solid films, with regards to transmission in a specified spectral range, is encapsulated in Table 1. Special emphasis was accorded to the transparency across different spectral ranges, namely, visible, near-infrared (IR), mid-IR, and THz.

Our investigations divulged that TPX consistently exhibited the highest transparency across all spectral ranges. However, when comparing SF-DNA and PTFE, we noticed comparable transmission characteristics. For equivalent film thickness, both demonstrated similar transmission properties in the THz range. Nevertheless, SF-DNA surpassed PTFE in terms of transparency in the visible and near-IR spectrum. Furthermore, the highest absorption of SF-DNA was found to occur in the mid-IR range, thus earmarking SF-DNA as a viable candidate for a painting material designed to obstruct thermal images. The superior transmittance of our SF-DNA in the visible and near IR, in comparison to PTFE, underscores its prospective utility as a dual window material for near IR and THz applications.

Cyclic olefin copolymer (TOPAS) is also known for its biocompatibility and high transmittance across the UV, visible, and THz ranges[59,60], similar to DNA films. However, DNA films offer distinct advantages, such as tunable optical properties, ease of functionalization, and natural compatibility with biological systems. Owing to its advantageous properties, SF-DNA films could serve as the primary optical material for THz and near IR, especially in applications where biocompatibility is of paramount importance.

With regard to near-IR applications, the [silica MMF]-[SF-DNA MMF]-[silica MMF] structure depicted in Figure 6 possesses the capacity to couple light with external factors such as temperature, humidity, and biochemical substances. Further refinements could potentially materialize a multimodal microscopic DNA-based waveguide sensor, a development we are ardently pursuing.

An additional noteworthy advantage of SF-DNA over other materials resides in its processing temperature of ~ 30 °C for solidification, which enables deposition over soft materials. In stark contrast, TPX and PTFE necessitate a processing temperature at least an order of magnitude higher, thereby constraining the selection of substrates.

We have successfully developed fabrication methodologies for both nanometer and micron scale surfactant-free DNA solid films, culminating in three distinct constructs: DNA films on substrates, freestanding DNA films, and a cylindrical DNA construct held in place between two optical fibers. A comprehensive exploration of the optical properties of these constructs was conducted across an expansive spectral range, encompassing wavelengths from the ultraviolet to the terahertz range. This included an analysis of both transmittance and refractive index. In the nanometer-scale DNA films deposited on Si wafers, we found significantly high birefringence in the order of 10^{-2} for the film thickness of 137 nm. The solid DNA cylinder between two optical fibers showed a propagation loss of 6.7 ~ 10.5 dB/mm in the near-IR spectra range of 1200 to 1600 nm, enabling application as a compact biochemical sensor. SF-DNA solid films demonstrated a unique dual-band transparency within the near-infrared and terahertz ranges. A substantial transmittance exceeding 75% was achieved within the near-infrared spectral ranges of 1270 to 1390 nm and 1580 to 1870 nm, as well as within the 0.22 to 0.64 terahertz range. Additionally, the SF-DNA solid films demonstrated a promising capacity as a mid-infrared absorbing material. This latter property implies potential application in thermal sensing impediment.

Data availability

The datasets used and/or analysed during the current study are available from the corresponding author on reasonable request.

Received: 29 January 2024; Accepted: 28 October 2024
Published online: 21 November 2024

References

1. Jd, W. Molecular structure of nucleic acids: A structure for deoxyribose nucleic acid. *Nature* **171**, 737–738 (1953).
2. Kawabe, Y., Wang, L., Horinouchi, S. & Ogata, N. Amplified spontaneous emission from fluorescent-dye-doped DNA–surfactant complex films. *Adv. Mater.* **12**, 1281–1283 (2000).
3. Kawabe, Y., Wang, L., Koyama, T., Horinouchi, S. & Ogata, N. in *Linear, Nonlinear, and Power-Limiting Organics*. 369–376 (International Society for Optics and Photonics).
4. Khazaeinezhad, R. et al. Ultrafast nonlinear optical properties of thin-solid DNA film and their application as a saturable absorber in femtosecond mode-locked fiber laser. *Sci. Rep.* **7**, 41480 (2017).
5. Hagen, J. A., Li, W., Steckl, A. & Grote, J. Enhanced emission efficiency in organic light-emitting diodes using deoxyribonucleic acid complex as an electron blocking layer. *Applied Physics Letters* **88**, 171109 (2006).
6. Sun, Q. et al. highly efficient quantum-dot light-emitting diodes with DNA− CTMA as a combined hole-transporting and electron-blocking layer. *Acs Nano* **3**, 737–743 (2009).
7. Heckman, E. M. et al. DNA biopolymer conductive cladding for polymer electro-optic waveguide modulators. *Appl. Phys. Lett.* **98**, 54 (2011).
8. Singh, B., Sariciftci, N. S., Grote, J. G. & Hopkins, F. K. Bio-organic-semiconductor-field-effect-transistor based on deoxyribonucleic acid gate dielectric. *J. Appl. Phys.* **100**, 024514 (2006).
9. Kulkarni, A. et al. A novel nanometric DNA thin film as a sensor for alpha radiation. *Sci. Rep.* **3**, 1–5 (2013).
10. Hong, S. et al. Thermo-optic characteristic of DNA thin solid film and its application as a biocompatible optical fiber temperature sensor. *Opt. Lett.* **42**, 1943–1945 (2017).
11. Grote, J. G. et al. DNA photonics [deoxyribonucleic acid]. *Mol. Cryst. Liquid Cryst.* **426**, 3–17 (2005).
12. Yumusak, C., Singh, T. B., Sariciftci, N. & Grote, J. Bio-organic field effect transistors based on crosslinked deoxyribonucleic acid (DNA) gate dielectric. *Appl. Phys. Lett.* **95**, 341 (2009).
13. Jeong, H., Bjorn, P., Hong, S., Cheon, S. & Oh, K. Irreversible denaturation of DNA: a method to precisely control the optical and thermo-optic properties of DNA thin solid films. *Photonics Res.* **6**, 918–924 (2018).
14. Paulson, B. et al. Optical dispersion control in surfactant-free DNA thin films by vitamin B 2 doping. *Sci. Rep.* **8**, 1–10 (2018).
15. Samoc, A., Miniewicz, A., Samoc, M. & Grote, J. G. Refractive-index anisotropy and optical dispersion in films of deoxyribonucleic acid. *J. Appl. Polym. Sci.* **105**, 236–245 (2007).
16. Gnapareddy, B. et al. Chemical and physical characteristics of doxorubicin hydrochloride drug-doped salmon DNA thin films. *Sci. Rep.* **5**, 1–9 (2015).
17. Herrmann, M., Norizawa, K., Tabata, H. & Kawai, T. in *2005 Joint 30th International Conference on Infrared and Millimeter Waves and 13th International Conference on Terahertz Electronics*. 475–476 (IEEE).
18. Sönmezoğlu, S. & Sönmezoğlu, Ö. A. Optical and dielectric properties of double helix DNA thin films. *Mater. Sci. Eng.: C* **31**, 1619–1624 (2011).
19. Arasu, V. et al. Thickness, morphology, and optoelectronic characteristics of pristine and surfactant-modified DNA thin films. *J. Phys. D: Appl. Phys.* **50**, 415602 (2017).
20. Jung, W. et al. Cationic lipid binding control in DNA based biopolymer and its impacts on optical and thermo-optic properties of thin solid films. *Opt. Mater. Express* **7**, 3796–3808 (2017).
21. Cheng, H.-R. & Jiang, N. Extremely rapid extraction of DNA from bacteria and yeasts. *Biotechnol. Lett.* **28**, 55–59 (2006).
22. Sahu, S. K., Thangaraj, M. & Kathiresan, K. DNA extraction protocol for plants with high levels of secondary metabolites and polysaccharides without using liquid nitrogen and phenol. *International Scholarly Research Notices* **2012** (2012).
23. Manchester, K. L. Use of UV methods for measurement of protein and nucleic acid concentrations. *Biotechniques* **20**, 968–970 (1996).
24. Zhang, L. & Dong, J. High-rate tunable ultrasonic force regulated nanomachining lithography with an atomic force microscope. *Nanotechnology* **23**, 085303 (2012).
25. Kubacki, E. The dirt on cleaning optics. *Photonics Spectra* **40**, 56 (2006).
26. Long, W. *et al.* in *CLEO: Science and Innovations*. CME1 (Optical Society of America).
27. Long, W., Zou, W., Li, X. & Chen, J. DNA optical nanofibers: preparation and characterization. *Opt. Express* **20**, 18188–18193 (2012).
28. Amin, R., Kulkarni, A., Kim, T. & Park, S. H. DNA thin film coated optical fiber biosensor. *Curr. Appl. Phys.* **12**, 841–845 (2012).
29. Kwon, Y.-W., Lee, C. H., Choi, D.-H. & Jin, J.-I. Materials science of DNA. *J. Mater. Chem.* **19**, 1353–1380 (2009).
30. Workman, J. & Weyer, L. *Practical Guide and Spectral Atlas for Interpretive Near-Infrared*. (CRC, 2012).
31. Poch, O. et al. Remote sensing of potential biosignatures from rocky, liquid, or icy (exo) planetary surfaces. *Astrobiology* **17**, 231–252 (2017).
32. Giedraityte, Z., Sainio, J., Hagen, D. & Karppinen, M. Luminescent metal-nucleobase network thin films by atomic/molecular layer deposition. *J. Phys. Chem. C* **121**, 17538–17545 (2017).
33. Kim, M. et al. Optical properties of nucleobase thin films as studied by attenuated total reflection and surface-enhanced Raman spectroscopy. *Opt. Mater.* **78**, 531–537 (2018).
34. Breazu, C. et al. Nucleobases thin films deposited on nanostructured transparent conductive electrodes for optoelectronic applications. *Sci. Rep.* **11**, 1–15 (2021).
35. Liu, Y., Hsieh, J. & Tung, S. Extraction of optical constants of zinc oxide thin films by ellipsometry with various models. *Thin Solid Films* **510**, 32–38 (2006).
36. Ong, H. & Chang, R. P. Optical constants of wurtzite ZnS thin films determined by spectroscopic ellipsometry. *Appl. Phys. Lett.* **79**, 3612–3614 (2001).
37. Nir, E., Kleinermanns, K. & de Vries, M. S. Pairing of isolated nucleic-acid bases in the absence of the DNA backbone. *Nature* **408**, 949–951 (2000).
38. Hamada, S. & Murata, S. Substrate-Assisted Assembly of Interconnected Single-Duplex DNA Nanostructures. *Angew. Chemie* **121**, 6952–6955 (2009).
39. Keller, D., Bustamante, C. & Keller, R. W. Imaging of single uncoated DNA molecules by scanning tunneling microscopy. *Proc. Natl. Acad. Sci.* **86**, 5356–5360 (1989).
40. Weidlich, T., Lindsay, S. & Rupprecht, A. The optical properties of Li-and Na-DNA films. *Biopolymers: Original Res. Biomol.* **26**, 439–453 (1987).
41. Hebda, E. et al. Optical properties of thin films of DNA-CTMA and DNA-CTMA doped with Nile blue. *Mol. Cryst. Liquid Cryst.* **556**, 309–316 (2012).
42. Sugimoto, Y. *et al.* Low propagation loss of 0.76 dB/mm in GaAs-based single-line-defect two-dimensional photonic crystal slab waveguides up to 1 cm in length. *Opt. Express* **12**, 1090–1096 (2004).
43. Zimmermann, J. et al. Photonic crystal waveguides with propagation losses in the 1 dB/ mm range. *J. Vacuum Sci. Technol. B: Microelectron. Nanometer Struct. Process. Meas. Phenomena* **22**, 3356–3358 (2004).
44. Goto, T. et al. Propagation loss measurement for surface plasmon-polariton modes at metal waveguides on semiconductor substrates. *Appl.Phys. Lett.* **84**, 852–854 (2004).
45. Wang, X. & Son, A. Effects of pretreatment on the denaturation and fragmentation of genomic DNA for DNA hybridization. *Environ. Sci.: Processes Impacts* **15**, 2204–2212 (2013).
46. Soref, R. Mid-infrared photonics in silicon and germanium. *Nature Photonics* **4**, 495–497 (2010).

47. Gulmine, J., Janissek, P., Heise, H. & Akcelrud, L. *Polyethylene characterization by FTIR. Polymer testing* **21**, 557–563 (2002).
48. Neu, J. & Schmuttenmaer, C. A. Tutorial: An introduction to terahertz time domain spectroscopy (THz-TDS). *J. Appl. Phys.* **124**, 231101 (2018).
49. Krotkus, A. Semiconductors for terahertz photonics applications. *J. Phys. D: Appl. Phys.* **43**, 273001 (2010).
50. Keun Yoo, H. et al. Organic conjugated material-based broadband terahertz wave modulators. *Appl. Phys. Lett.* **99**, 061108 (2011).
51. Globus, T. et al. Submillimeter-wave Fourier transform spectroscopy of biological macromolecules. *J. Appl. Phys.* **91**, 6105–6113 (2002).
52. Globus, T. R. et al. THz-spectroscopy of biological molecules. *J. Biol. Phys.* **29**, 89–100. https://doi.org/10.1023/a:1024420104400 (2003).
53. Jin, Y.-S., Kim, G.-J. & Jeon, S.-G. Terahertz dielectric properties of polymers. *J. Korean Phys. Soc.* **49**, 513–517 (2006).
54. Yasuda, H. & Hosako, I. in *2007 IEEE/MTT-S International Microwave Symposium.* 1125–1128 (IEEE).
55. Tydex, J.
56. Lytle, J. D., Wilkerson, G. W. & Jaramillo, J. G. Wideband optical transmission properties of seven thermoplastics. *Appl. Opt.* **18**, 1842–1846 (1979).
57. Podzorov, A. & Gallot, G. Low-loss polymers for terahertz applications. *Appl. Opti* **47**, 3254–3257 (2008).
58. Galante, A., Galante, O. & Campos, L. Study on application of PTFE, FEP and PFA fluoropolymers on radiation dosimetry. *Nucl. Instrum. Methods Phys. Res. Sect. A: Accelerators Spectrometers Detectors Assoc. Equip.* **619**, 177–180 (2010).
59. Khanarian, G. & Celanese, H. Optical properties of cyclic olefin copolymers. *Opt. Eng.* **40**, 1024–1029 (2001).
60. Wollack, Edward J., et al. Far-infrared properties of cyclic olefin copolymer. *Opt. Lett.* **45**, 780–783 ,(2020).

Acknowledgements

This work was supported by the National Research Foundation of Korea (NRF) grant funded by the Korea government (MSIT) (No. 2019R1A2C2011293).

Author contributions

Hayoung Jeong, Seunguk Cheon**:** Conceptualization, Data curation, Formal analysis, Visualization, Validation, Writing paper. Yong Soo Lee, Marjan Ghasemi, Soeun Kim, Chul Kang, Inhee Maeng, Seongjin Hong: Investigation, Organization. Kyunghwan Oh: Methodology, Organization, Funding acquisition, Review, editing.

Declarations

Competing interests

The authors declare no competing financial interests.

Additional information

Correspondence and requests for materials should be addressed to K.O.

Reprints and permissions information is available at www.nature.com/reprints.

Publisher's note Springer Nature remains neutral with regard to jurisdictional claims in published maps and institutional affiliations.